Article:

Wernli, H, Boettcher, M, Joos, H et al. (2 more authors) (2016) A trajectory-based classification of ERA-Interim ice clouds in the region of the North Atlantic storm track. Geophysical Research Letters, 43 (12). pp. 6657-6664. ISSN 1944-8007

https://doi.org/10.1002/2016GL068922

A trajectory-based classification of ERA-Interim ice clouds in the region of the North Atlantic storm track

H. Wernli[1], M. Boettcher[1], H. Joos[1], A. K. Miltenberger[2], and P. Spichtinger[3]

Corresponding author: H. Wernli, Institute for Atmospheric and Climate Science, ETH Zurich, Universitätstrasse, 8092 Zürich, Switzerland. (heini.wernli@env.ethz.ch)

[1]Institute for Atmospheric and Climate Science, ETH Zurich, Zurich, Switzerland.

[2]School of Earth and Environment, University of Leeds, Leeds, United Kingdom.

[3]Institute for Atmospheric Physics, Johannes Gutenberg University, Mainz, Germany.

A two-type classification of ice clouds (cirrus) is introduced, based on the liquid and ice water content, LWC and IWC, along air parcel backward trajectories from the clouds. In-situ cirrus has no LWC along the trajectory segment containing IWC; it forms via nucleation from the gas phase. In contrast, liquid-origin cirrus has both LWC and IWC along their backward trajectories; it forms via lifting from the lower troposphere and freezing of mixed-phase clouds. This classification is applied to 12 years of ERA-Interim ice clouds in the North Atlantic region. Between $400-500$ hPa more than 50% are liquid-origin cirrus, whereas this frequency decreases strongly with altitude (<10% at 200 hPa). The relative frequencies of the two categories vary only weakly with season. More than 50% of in-situ cirrus occur on top of liquid-origin cirrus, indicating that they often form in response to the strong lifting accompanying the formation of liquid-origin cirrus.

1. Introduction

Clouds in the tropopause region consisting exclusively of ice crystals (ice clouds or cirrus clouds) are, as all other clouds, important modulators of the Earth's energy budget. They scatter incoming solar radiation back to space (albedo effect) and trap terrestrial infrared emissions (greenhouse effect). In contrast to liquid water clouds, for ice clouds both effects are of the same order of magnitude, modulated by the shape and size of ice crystals [e.g., *Wendisch et al.,* 2007]. The general net effect of cirrus clouds on the radiation budget is not well known. A transition between net warming and cooling can occur due to variations in number concentrations, ice water content and shapes [*Zhang et al.,* 1999], or in response to the time of day and the nucleation mechanism [*Joos et al.,* 2014]. Evaluations of ISCCP satellite data indicated a top of atmosphere net warming of cirrus clouds [*Chen et al.,* 2000]. However, the classification of cirrus clouds was carried out using optical depth only and the resolution of these satellite data was rather coarse. In-situ observations reveal a huge variability of ice cloud properties in the tropopause region. Ice crystal number concentration and sizes vary over orders of magnitudes [*Krämer et al.,* 2009] and ice water content (IWC) values also show a huge variability [e.g., *Luebke et al.,* 2013, and references therein]. These strongly varying cirrus properties are crucially determined by the formation pathway of ice crystals, which in turn is very likely related to the driving weather system.

Cirrus classification schemes, mainly applied in the tropics, distinguish for instance between ice clouds linked to the outflow of deep convective systems and those formed in-situ in the upper troposphere [*Massie et al.,* 2002; *Luo and Rossow,* 2004]. For the convective scenario, it is likely that a lot of ice particles in the cold anvil cirrus formed via freezing of liquid cloud droplets in the mixed-phase part of the convective cloud, which is fundamentally different from the in-situ ice formation in the second scenario. Mid-latitude cirrus clouds occur under an even larger diversity of weather systems, including, e.g., frontal clouds in the storm track region, deep convection, and orographic clouds [*Sassen and Campbell,* 2001; *Berry and Mace,* 2013; *Muhlbauer et al.,* 2014]. In terms of the prevailing large-scale flow conditions, *Gierens and Brinkop* [2012] emphasized that ice supersaturation in mid-latitudes preferentially occurs in upper-level ridges. Other classifications are based on the clouds' optical depth [e.g., *Hoareau et al.,* 2013] or their vertical IWC profile [*Feofilov et al.,* 2015]. Such classifications are meteorologically interesting, but with respect to the physical properties of ice clouds, a classification according to the formation pathway using thermodynamic characteristics might be more meaningful.

Therefore, this study uses the following two-fold classification of ice clouds, which considers the thermodynamic characteristics of cirrus air parcels and uses backward trajectories to distinguish between so-called liquid-origin and in-situ cirrus clouds:

- Liquid-origin cirrus: ice crystals form via freezing of previously formed large cloud droplets (i.e., of droplets with a diameter larger than $1\,\mu$m). In terms of freezing processes [e.g., *Hoose and Möhler,* 2012; *Vali et al.,* 2015] this can occur via immersion or contact freezing. At temperatures $T > -38°$C, the freezing occurs close to thermodynamic equilibrium with respect to water, i.e., close to water saturation, and the three phases vapor, liquid water and ice coexist. Therefore for such a cloud there is a period along the backward trajectory during which LWC co-occurs with IWC. Once such an air parcel reaches a temperature below about −38°C, all water droplets can be assumed to freeze spontaneously.

- In-situ cirrus: ice crystals form via nucleation that does not involve large cloud droplets, e.g., via heterogeneous nucleation on the surface of solid particles (deposition freezing) [e.g., *Hoose and Möhler,* 2012] or homogeneous freezing of supercooled aqueous solution droplets (homogeneous nucleation) [e.g., *Koop et al.,* 2000]. In this case the air parcel never reaches saturation with respect to water during the ascent, but reaches high supersaturation with respect to ice at temperatures below −38°C. For this type of clouds no LWC exists along the backward trajectory segment containing IWC (note that the potentially existing aqueous solution droplets are too small to be considered as cloud droplets and do not contribute to LWC).

For both categories diffusional growth will drive the clouds towards the stable equilibrium, i.e., saturation with respect to ice. External forcings such as adiabatic cooling due to upward motion might lead to dynamic steady states far away from thermodynamic equilibrium [see, e.g., *Korolev and Mazin,* 2003; *Krämer et al.,* 2009; *Spichtinger,* 2014].

These two categories of liquid-origin and in-situ cirrus have been introduced recently by *Krämer et al.* [2016] and *Luebke et al.* [2016], who performed a detailed analysis of aircraft observations and found higher values of IWC, ice crystal concentration and ice crystal size for the category of liquid-origin cirrus. Their observational results, indicating that ice clouds originating from the two pathways have different microphysical and macrophysical properties, motivate the systematic trajectory-based climatological analysis in this study. Examples for liquid-origin cirrus are anvil clouds in thunderstorms and warm conveyor belts (WCBs) associated with extratropical cyclones. WCBs are moist ascending airstreams from the boundary layer up to the upper troposphere [*Browning,* 1990; *Wernli and Davies,* 1997] and lead to the formation of ice crystals after forming water droplets in the middle troposphere. In addition, the strong ascent of the WCB is pushing upper tropospheric air masses upward, leading to gentle ascent above the WCB in the cold temperature regime, which can trigger the formation of a layer of in-situ cirrus on top of the liquid-origin cirrus. *Spichtinger et al.* [2005] described such a situation in a case study of a North Atlantic cyclone.

Our trajectory-based classification considers the scenario that ice crystals form in lifted air parcels, which cool adiabatically and reach supersaturation with respect to water or ice. The processes of sedimentation of ice crystals and turbulent mixing have a weak influence on the main formation mechanism of ice along trajectories and therefore the classification in in-situ and liquid-origin clouds. The use of air parcel trajectories for cirrus cloud studies is not new. In many former studies box models along trajectories were used to investigate microphysical properties of ice clouds (typically in-situ cirrus) [e.g., *Haag and Kärcher,* 2004; *Hoyle et al.,* 2005; *Spichtinger and Krämer,* 2013; *Kienast-Sjögren et al.,* 2015]. Trajectory calculations using large-scale wind fields were also used, for instance, to quantify the duration of ice-supersaturation along trajectories in the upper troposphere [*Irvine et al.,* 2014], to investigate potential ice-cloud formation mechanisms in air parcels originating from the major dust emission regions [*Wiacek et al.,* 2010], and to estimate the water vapor transport across the tropical tropopause resulting from cirrus dehydration [*Fueglistaler et al.,* 2005]. The novel aspect in this study is that trajectories are used for a climatological cirrus classification in the extratropics, distinguishing two fundamental formation pathways (liquid-origin vs. in-situ origin). This setup is explained in Section 2. Section 3 then presents results of winter and summer season climatologies of the two ice cloud categories from January 2000 to December 2012 in the region of the North Atlantic storm track, using ERA-Interim reanalyses [*Dee et al.,* 2011]. Section 4 provides two exemplary case studies and Section 5 discusses the potential relevance of the classification.

2. Methodology

All calculations in this study are based on ERA-Interim wind fields, temperature, cloud ice and liquid water content, IWC and LWC, respectively, interpolated to a regular 1° by 1° grid on the 60 original hybrid sigma-pressure levels. The Lagrangian analysis tool LAGRANTO [*Wernli and Davies,* 1997; *Sprenger and Wernli,* 2015] is used to calculate backward trajectories every 6 hours from starting points where a pure ice cloud is present (IWC $> 0.1\,\mathrm{mg\,kg^{-1}}$ and LWC $< 0.01\,\mathrm{mg\,kg^{-1}}$). The starting points are set horizontally on the 1° by 1° grid and vertically on 11 pressure levels, every 40 hPa between 100 and 500 hPa in the North Atlantic / European region extending from 100°W to 40°E and from 30 to 80°N. The trajectories are calculated five days backward in time, assuming that ice clouds in a specific air parcel hardly ever exist for longer and that this duration therefore allows for a meaningful categorization of in-situ and liquid-origin ice clouds. LAGRANTO calculates kinematic trajectories using the three-dimensional wind field with the vertical motion in $\mathrm{Pa\,s^{-1}}$.

The categorization algorithm then considers for every trajectory the backward segment until the air parcel contains virtually no ice (IWC $< 0.1\,\mathrm{mg\,kg^{-1}}$). The length of this trajectory segment can vary between six hours and five days. In the schematic Fig. 1 the length of this segment is 48 h for both example trajectories in panels (a) and (b). It is then verified whether the air parcel contained liquid cloud water (LWC $> 0.01\,\mathrm{mg\,kg^{-1}}$) at any time during this time period. If this is not the case (Fig. 1a), then the considered trajectory represents an in-situ ice cloud, and if this is the case (Fig. 1b), then the trajectory belongs to the category of liquid-origin ice clouds. Trajectories that ascend as part of a WCB represent a special subcategory of liquid-origin ice clouds. These trajectories are additionally characterized by an ascent of at least 600 hPa in 48 hours [*Joos and Wernli,* 2012; *Madonna et al.,* 2014] during any of the 48-hour intervals along the 5-day backward trajectories.

This simple algorithm is applied to all the about 350 million cirrus trajectories in the 12 years of ERA-Interim data, and since the trajectories were started every 6 hours on a regular grid (see above), a three-dimensional Eulerian field can be constructed every 6 hours, which indicates at every grid point the identified ice cloud category. From these fields it is then straightforward to calculate climatological frequency fields for the different categories (Section 3), and to visualize the spatial distribution of the categories for specific case studies (Section 4).

Before discussing the results, it is important to mention some limitations of our approach to diagnose ice cloud properties with air parcel trajectories using ERA-Interim data: (i) ice clouds in ERA-Interim are poorly constrained by observations, and they are produced by rather simplistic cloud microphysics, and (ii) trajectory calculations with ERA-Interim wind fields are based on grid-scale winds, which cannot resolve the rapid vertical motion in deep convective clouds. Here we discuss the first of these limitations; the impact of the second one on our classification is briefly addressed in the final section. The thermodynamic cloud phase in ERA-40 and ERA-Interim is parameterized simply as a function of temperature, with pure ice clouds below −23°C, and mixed-phase clouds between −23°C and 0°C. According to *Dee et al.* [2011], the representation of clouds in the here used ERA-Interim dataset is improved compared to ERA-40, in particular by introducing ice supersaturation, which delays the formation of ice clouds. Convection is parameterized, and water detrained from convective clouds is handed over to the prognostic cloud scheme [*ECMWF,* 2007]. This implies that some of the ERA-Interim ice clouds at temperatures below −23°C are produced by detrainment of ice from deep convective clouds. Despite the simplicity of the ice cloud microphysics, climatological comparisons indicate a fairly good agreement with satellite observations, in particular in the extratropical storm track regions at temperatures below −30°C [*Weidle and Wernli,* 2008], i.e., in the main region of interest for this study. This is confirmed by *Ma et al.* [2012] who showed similar values of seasonal mean IWC at 300 and 500 hPa in CloudSat and ERA-Interim in the storm track regions (but not in the tropics and below 500 hPa).

Super-cooled liquid water can exist at temperatures down to about −40°C. Thus, in the regime $-40° < T < -23°$C we might overestimate the number of in-situ formed ice clouds. In this temperature regime in reality a super-cooled water cloud may form first and ice crystals are formed later, which would constitute a liquid-origin ice cloud. However, ERA-Interim data do not include such events because of the simple implemented ice cloud parameterization. From in-situ observations of stratiform mixed-phase clouds as analyzed by *Boudala et al.* [2004] we know that the liquid cloud fraction in this temperature regime is usually smaller than 20%. Thus, we conclude that the maximum overestimation of in-situ origin ice clouds on the expense of liquid-origin ice clouds is smaller than 20%, and this number is decreasing with decreasing temperature, see, e.g., Fig. 4 in *Boudala et al.* [2004]. Despite these limitations, the quality of ERA-Interim is sufficient for a first climatological application of the trajectory-based cirrus categorization.

3. Climatological results

Figure 2 presents the climatological distribution of in-situ and liquid-origin ice clouds at two pressure levels (300 and 220 hPa, respectively) over the North Atlantic in winter and summer. The 300 hPa level has been chosen because it is close to the level with maximum ice cloud frequencies (see below) and the 220 hPa level because it is on average located in the stratosphere (over the North Atlantic) and therefore contains ice clouds mainly during high-pressure conditions associated with an elevated tropopause. Ice cloud frequency fields on other levels between 180 and 500 hPa and in all seasons are shown in the supplemental material (Figs. S1, S2).

At 300 hPa in winter (Fig. 2c) the geographical distribution of the two types of ice clouds is fairly similar with higher frequencies of in-situ ice clouds. In winter both types reach highest frequencies over the central North Atlantic near 40°N, with peak values larger than 30% for in-situ (red contours) and 20% for liquid-origin cirrus (filled colors). A frequency value of, e.g., 20% indicates that in 20% of all 6-hourly time steps an ice cloud of this category is present in the ERA-Interim dataset at this location and vertical level. Since the total ice cloud frequency corresponds to the sum of these two categories, we find peak values of ice cloud frequency exceeding 50% at 300 hPa in the central North Atlantic. The contours of 20% in-situ and 10% liquid-origin ice cloud frequencies, respectively, correspond quite nicely to the North Atlantic storm track region characterized by cyclone frequencies of about 20% (see Fig. 4a in *Wernli and Schwierz* [2006]). The region near 40°W, $35-60$°N with high frequencies of liquid-origin ice clouds agrees qualitatively with the main outflow region of WCBs (see Fig. 4f in *Madonna et al.* [2014]). Over eastern North America the frequency of liquid-origin ice clouds reaches more than 10%; similar values can be found over most parts of western and northern Europe whereas over the UK the values are slightly larger. Over the Mediterranean the winter ice cloud frequencies at 300 hPa are lower than 10% for liquid-origin and 20-30% for in-situ cirrus. At 220 hPa (Fig. 2a), the frequencies of liquid-origin ice clouds is strongly reduced and are mainly confined to the North Atlantic region. Maximum values over the central North Atlantic are again above 30% for in-situ and only about 6% for liquid-origin ice clouds.

In summer (Figs. 2b,d) the frequency patterns are more complex and, e.g., for liquid-origin ice clouds at 300 hPa show three maxima, one pronounced ($> 25\%$) along the US east coast at 35°N, and two weaker ones (about 15%) over Labrador and Scandinavia (Fig. 2d). In-situ ice clouds at the same level, however, reveal a pronounced peak of 50% over the Alps. Considering the seasonal mean precipitation fields (supplemental Fig. S3) indicates that this is a region where parameterized convection in ERA-Interim is intense. At 220 hPa, liquid-origin ice clouds occur with frequencies larger than 10% in the western

North Atlantic and in-situ ice clouds are very frequent in the same region (> 50%) as well as over Central and Eastern Europe (20-40%) (Fig. 2b). In summer, the frequency of North Atlantic WCBs is low [*Madonna et al., 2014*] and therefore the WCB outflow pattern (Fig. 5f in *Madonna et al.* [2014]) does not co-occur with an ice cloud frequency hotspot. Similarly, the qualitative agreement between the storm track (Fig. 4c in *Wernli and Schwierz* [2006]) and the ice cloud frequency pattern is weaker than in winter. The secondary maxima near Labrador and Scandinavia coincide with active cyclone regions, but not so the main ice cloud peaks along the US east coast (in-situ and liquid-origin) and over the Alps (mainly in-situ), which however both agree with ERA-Interim convective activity (Fig. S3). Note that the regions with the highest cirrus frequencies in winter (central North Atlantic near 40°N) and summer (band along the U.S. east coast) agree qualitatively very well with the satellite-derived high cloud climatology by *Stubenrauch et al.* [2010, their Fig. 6].

Figure 3 shows vertical profiles of the domain-averaged frequency distributions, again for summer and winter. In winter, the total ice cloud frequency (sum of in-situ and liquid-origin) is largest between 350 and 400 hPa (about 40%, with averaged T of about -40°C). In summer, similar values occur a bit higher, between 300 and 350 hPa, again at about $T = -40$°C. Not surprisingly, given the generally higher temperatures, ice cloud frequencies are strongly reduced in summer below 400 hPa. Although in-situ ice clouds are slightly less frequent than liquid-origin ice clouds below 400 hPa, they become more than twice as abundant above 300 hPa and reach near totality above 200 hPa (i.e., at $T < -55$°C). This is true for both seasons. Domain mean maxima of liquid-origin frequencies reach just above 20% at 420 hPa in winter and about 17% at 340-380 hPa in summer. The conditional frequency of liquid-origin ice cloud (dashed blue line) peaks at more than 50% around 450 hPa and then decreases almost linearly to zero by 140 hPa (irrespective of season). Finally, we note that liquid-origin ice clouds with a WCB ascent (green line for category 3) occur between 200 and 400 hPa in winter with absolute frequency maxima of about 1% and relative frequency maxima of about 2% near 300 hPa. The fairly frequent liquid-origin ice clouds below 400 hPa do not belong to this category because of the 600 hPa ascent criterion required for WCBs. Note that the fairly frequent liquid-origin ice clouds below 400 hPa do not belong to this category because of the 600 hPa ascent criterion required for WCBs. As additional information, the supplemental Fig. S4 shows a temperature histogram for the three categories. Interestingly, at $T = -30°$C in-situ and liquid-origin ice clouds are equally frequent (in the considered North Atlantic region) and liquid-origin ice clouds with a WCB ascent are most frequent at fairly low temperatures of about $-50°$C.

4. Case studies and the vertical arrangement of the two categories

Figure 4 shows two case studies to provide an impression of how the different ice cloud categories can be spatially related in situations with a strong WCB outflow associated with a North Atlantic cyclone. The first case has been investigated by *Spichtinger et al.* [2005] and reveals a large ice cloud at 300 hPa extending over large parts of the eastern North Atlantic and Western Europe (Figs. 4a,b). A liquid-origin ice cloud with a WCB ascent is located over the North Sea, embedded in a liquid-origin ice cloud with a weaker ascent, which in turn is embedded in an in-situ ice cloud and other patches of liquid-origin ice clouds. The vertical cross section shows nicely how spatially separated ice clouds of liquid-origin between 500 and 250 hPa are enclosed by an even larger in-situ ice cloud reaching up to 160 hPa. A similar situation occurs for the second case with the WCB outflow over Scandinavia studied by *Joos and Wernli* [2012]. Also here, a liquid-origin ice cloud associated with a WCB between about 250 and 350 hPa is horizontally and vertically embedded first in a massive liquid-origin ice cloud and then topped by a thinner in-situ ice cloud (Figs. 4c,d). It is remarkable that in both cases, the WCB-related parts of the ice clouds extend to very low temperatures of about −50°C and −60°C, respectively.

These case studies show that large ice cloud features (e.g., on a satellite picture) can be composed of sub-entities with strongly contrasting formation mechanisms. This pattern is pronounced, e.g., near WCBs, where in-situ ice clouds form in layers covering the upper and lateral part of liquid-origin ice clouds. This layering has been proposed by *Spichtinger et al.* [2005]; dynamically it indicates that very strongly ascending WCB air masses are surrounded by less strongly ascending air masses (which however still originate from regions with mixed-phase clouds) and topped by weakly ascending air masses leading to the formation of in-situ cirrus. We applied a simple algorithm to the 12-year climatology discussed in Section 3 to quantify how often (i) a liquid-origin ice cloud grid point is topped by a connected in-situ ice cloud in the same column, and (ii) how often an in-situ ice cloud is topping a connected liquid-origin ice cloud. The statistical result is that in all seasons more than 80% of liquid-origin ice clouds are topped by an in-situ ice cloud, and more than 50% of the in-situ ice clouds have a liquid-origin ice cloud in the same column at a lower altitude. These high values indicate a strong dynamical linkage between the two cirrus categories and place the case study results in a more general context.

5. Conclusions

A trajectory-based ice cloud classification has been applied for the first time to a long-term data set with the aim to climatologically quantify the frequency of in-situ and liquid-origin ice clouds (Krämer et al., 2016; Luebke et al., 2016) at different pressure levels in the North Atlantic storm track region. The results show that (i) the two categories are about equally abundant between 500-400 hPa (i.e., at $T > -35°C$ in DJF and $> -25°C$ in JJA); (ii) at the level where ice clouds are most frequent (about 300 hPa; at $T \simeq -48°C$ in DJF and $\simeq -40°C$ in JJA) about 30% of all cirrus are liquid-origin; and (iii) above 200 hPa ($T < -60°C$) liquid-origin frequencies are below 10%. Seasonal variability is large for the spatial distribution of cirrus, but much smaller for the domain-averaged characteristics of the two categories.

During the summer season, peaks of in-situ cirrus occurrence in our diagnostic are co-located with convective activity along the US east coast and over Central Europe. This reveals an important caveat of our analysis, which is based on trajectories calculated with ERA-Interim winds. Given the spatial and temporal resolution of these fields, it is clear that the trajectories cannot capture the rapid vertical motion and the transition from mixed-phase to ice clouds associated with deep convection. Therefore, most likely, many convection-related liquid-origin ice clouds are erroneously classified here as in-situ ice clouds. A similar overestimation of in-situ ice clouds occurs due to the simple ice cloud scheme in ERA-Interim, as discussed in section 2. The values given for liquid-origin frequencies should therefore be regarded as lower estimates. Only trajectories calculated with very high-resolution data (e.g., from a convection-permitting model simulation, *Miltenberger et al.* [2013]) could help with this issue; however, no such dataset is currently available for a climatological time period.

Two case studies were shown to demonstrate the potential inhomogeneity and complexity of the formation pathways of synoptic scale ice clouds. What appears as "one large cloud" can be the result of a complex airflow, with WCB-like ascent from the boundary layer to the cirrus region embedded in air masses with (much) weaker ascent, in which ice clouds form in-situ. At the interface of the two cloud types, ice crystal sedimentation and cloud turbulence – two processes that are not captured by air parcel trajectories – could potentially alter the local cirrus characteristics and "confuse" the simple categorization. For example, large ice crystals formed in in-situ clouds can sediment into liquid-origin clouds. It will thus be very interesting to investigate in detail how the formation pathway categorization translates to variability of the ice clouds' characteristics, in addition to the results reported already in *Luebke et al.* [2016]. The trajectory-based classification introduced here has also been applied to all flights of the ML-Cirrus field experiment over the North Atlantic in 2014 [*Voigt et al.,* 2016]. The multi-faceted analysis of the measurements from this campaign in combination with the trajectory data might contribute to an improved understanding of archetypal pathways of ice cloud formation, their properties and radiative effects.

Acknowledgments. We thank Martin Krämer (FZ Jülich), Christiane Voigt and Ulrich Schumann (both DLR Oberpfaffenhofen) for very constructive discussions about this ice cloud classification, and the entire ML-Cirrus team for its interest in this work. We are also grateful for the constructive comments from Stephan Fueglistaler and an anonymous referee. The ERA-Interim data used in this study can be accessed from the ECMWF website (https://software.ecmwf.int/wiki/display/WEBAPI/Access+ECMWF+Public+Datasets). The results of this study are available from the authors upon request.

References

Berry, E., and G. G. Mace (2013), Cirrus cloud properties and the large-scale meteorological environment: relationships derived from A-Train and NCEP-NCAR reanalysis data, *J. Appl. Meteor. Clim.*, *52*, 1253-1276.

Boudala, F., G. A. Isaac, S. G. Cober, Q. Fu (2004), Liquid fraction in stratiform mixed-phase clouds from in situ observations. *Q. J. R. Meteorol. Soc.*, *130*, 2919-2931.

Browning, K. A. (1990), Organization of clouds and precipitation in extratropical cyclones. *Extratropical Cyclones: The Erik Palmén Memorial Volume*, C. W. Newton and E. O. Holopainen, Eds., Amer. Meteor. Soc., 129-153.

Chen, T., W. B. Rossow, and Y. C. Zhang (2000), Radiative effects of cloud-type variations, *J. Clim.*, *13*, 264286, 2000.

Dee, D. P., et al. (2011), The ERA-Interim reanalysis: Configuration and performance of the data assimilation system, *Q. J. R. Meteorol. Soc.*, *137*, 553-597.

ECMWF (2007), IFS documentation - Cy31r1. Part IV: Physical processes. European Centre for Medium-Range Weather Forecasts, Reading, UK, 155 pp.

Feofilov, A. G., C. J. Stubenrauch, and J. Delano (2015), Ice water content vertical profiles of high-level clouds: classification and impact on radiative fluxes, *Atmos. Chem. Phys.*, *15*, 12327-12344.

Fueglistaler, S., M. Bonazzola, P. H. Haynes, and T. Peter (2005), Stratospheric water vapor predicted from the Lagrangian temperature history of air entering the stratosphere in the tropics, *J. Geophys. Res.*, *110*, D08107, doi:10.1029/2004JD005516.

Gierens, K., and S. Brinkop (2012), Dynamical characteristics of ice supersaturated regions, *Atmos. Chem. Phys.*, *12*, 11933-11942.

Haag, W., and B. Kärcher (2004), The impact of aerosols and gravity waves on cirrus clouds at midlatitudes, *J. Geophys. Res.*, *109*, D12202, doi:10.1029/2004JD004579.

Hoareau, C., P. Keckhut, V. Noel, H. Chepfer, and J.-L. Baray (2013), A decadal cirrus clouds climatology from ground-based and spaceborne lidars above the south of France (43.9N5.7E), *Atmos. Chem. Phys.*, *13*, 6951-6963.

Hoose, C., and O. Möhler (2012), Heterogeneous ice nucleation on atmospheric aerosols: a review of results from laboratory experiments, *Atmos. Chem. Phys.*, *12*, 9817-9854.

Hoyle, C. R., B. P. Luo, and T. Peter (2005), The origin of high ice crystal number densities in cirrus clouds, *J. Atmos. Sci.*, *62*, 2568-2579.

Irvine, E. A., B. J. Hoskins, and K. P. Shine (2014), A Lagrangian analysis of ice-supersaturated air over the North Atlantic, *J. Geophys. Res. Atmos.*, *119*, 90-100.

Joos, H., and H. Wernli (2012), Influence of microphysical processes on the potential vorticity development in a warm conveyor belt: a case study with the limited area model COSMO, *Quart. J. Roy. Meteorol. Soc.*, *138*, 407-418.

Joos, H., P. Spichtinger, P. Reutter, and F. Fusina (2014), Influence of heterogeneous freezing on the microphysical and radiative properties of orographic cirrus clouds, *Atmos. Chem. Phys.*, *14*, 6835-6852.

Kienast-Sjögren, E., A. K. Miltenberger, B. P. Luo, and T. Peter (2015), Sensitivities of Lagrangian modeling of mid-latitude cirrus clouds to trajectory data quality, *Atmos. Chem. Phys.*, *15*, 7429-7447.

Koop, T., B. Luo, A. Tsias, and T. Peter (2000), Water activity as the determinant for homogeneous ice nucleation in aqueous solutions, *Nature*, *406*, 611-614.

Korolev, A., and I. Mazin, (2003), Supersaturation of water vapor in clouds, *J. Atmos. Sci.*, *60*, 2957-2974.

Krämer, M., et al. (2009), Ice supersaturations and cirrus cloud crystal numbers, *Atmos. Chem. Phys.*, *9*, 3505-3522.

Krämer, M., et al. (2016), A microphysics guide to cirrus clouds Part 1: Cirrus types, *Atmos. Chem. Phys.*, *16*, 3463-3483.

Luo, Z., and W. B. Rossow (2004), Characterizing tropical cirrus life cycle, evolution, and interaction with upper-tropospheric water vapor using Lagrangian trajectory analysis of satellite observations, *J. Climate*, *17*, 4541-4563.

Luebke, A. E., L. M. Avallone, C. Schiller, J. Meyer, C. Rolf, and M. Krämer (2013), Ice water content of Arctic, midlatitude, and tropical cirrus – Part 2: Extension of the database and new statistical analysis, *Atmos. Chem. Phys.*, *13*, 6447-6459, 2013.

Luebke, A. E., A. Afchine, A. Costa, J.-U. Grooß, J. Meyer, C. Rolf, N. Spelten, L. M. Avallone, D. Baumgardner, and M. Krämer (2016), The origin of midlatitude ice clouds and the resulting influence on their microphysical properties, *Atmos. Chem. Phys.*, *16*, 5793-5809.

Madonna, E., H. Wernli, H. Joos, and O. Martius (2014), Warm conveyor belts in the ERA-Interim data set (1979-2010). Part I: Climatology and potential vorticity evolution, *J. Climate*, *27*, 3-26.

Massie, S., A. Gettelman, W. Randel, and D. Baumgardner (2002), Distribution of tropical cirrus in relation to convection, *J. Geophys. Res.*, *107*, 4591, doi:10.1029/2001JD001293.

Miltenberger, A. K., S. Pfahl, and H. Wernli (2013), An online trajectory module (version 1.0) for the nonhydrostatic numerical weather prediction model COSMO, *Geosci. Model Dev.*, *6*, 1989-2004.

Muhlbauer, A., T. P. Ackerman, J. M. Comstock, G. S. Diskin, S. M. Evans, R. P. Lawson, and R. T. Marchand (2014), Impact of large-scale dynamics on the microphysical properties of midlatitude cirrus, *J. Geophys. Res. Atmos.*, *119*, 3976-3996.

Sassen, K., and J. R. Campbell (2001), A midlatitude cirrus cloud climatology from the facility for atmospheric remote sensing. Part I: Macrophysical and synoptic properties, *J. Atmos. Sci.*, *58*, 481-496.

Spichtinger, P. (2014), Shallow cirrus convection – a source for ice supersaturation, *Tellus A*, *66*, 19937, doi:10.3402/tellusa.v66.19937.

Spichtinger, P., and M. Krämer (2013), Tropical tropopause ice clouds: a dynamical approach to the mystery of low crystal numbers, *Atmos. Chem. Phys.*, *13*, 9801-9818.

Spichtinger, P., K. Gierens, and H. Wernli (2005), A case study on the formation and evolution of ice supersaturation in the vicinity of a warm conveyor belt's outflow region, *Atmos. Chem. Phys.*, *5*, 973-987.

Sprenger, M., and H. Wernli (2015), The LAGRANTO Lagrangian analysis tool – version 2.0, *Geosci. Model Dev.*, *8*, 2569-2586.

Stubenrauch, C. J., S. Cros, A. Guignard, and N. Lamquin (2010), A 6-year global cloud climatology from the Atmospheric InfraRed Sounder AIRS and a statistical analysis in synergy with CALIPSO and CloudSat, *Atmos. Chem. Phys.*, *10*, 7197-7214.

Vali, G., P. J. DeMott, O. Möhler, and T. F. Whale (2015), Technical Note: A proposal for ice nucleation terminology, *Atmos. Chem. Phys.*, *15*, 10263-10270.

Voigt, C., et al. (2016), ML-CIRRUS – The airborne experiment on natural cirrus and contrail cirrus with the high-altitude long-range research aircraft HALO, *Bull. Amer. Meteor. Soc.*, available online: http://journals.ametsoc.org/doi/abs/10.1175/BAMS-D-15-00213.1.

Weidle, F., and H. Wernli (2008), Comparison of ERA40 cloud top phase with POLDER-1 observations, *J. Geophys. Res.*, *113*, D05209, doi:10.1029/2007JD009234.

Wendisch, M., P. Yang, and P. Pilewskie (2007), Effects of ice crystal habit on thermal infrared radiative properties and forcing of cirrus, *J. Geophys. Res.*, *112*, D08201, doi:10.1029/2006JD007899.

Wernli, H., and H. C. Davies (1997), A Lagrangian-based analysis of extratropical cyclones. I: The method and some applications, *Quart. J. Roy. Meteor. Soc.*, *123*, 467-489.

Wernli, H., and C. Schwierz (2006), Surface cyclones in the ERA40 data set (1958- 2001). Part I: novel identification method and global climatology, *J. Atmos. Sci.*, *63*, 2486-2507.

Wiacek, A., T. Peter, and U. Lohmann (2010), The potential influence of Asian and African mineral dust on ice, mixed-phase and liquid water clouds, *Atmos. Chem. Phys.*, *10*, 8649-8667.

Zhang, Y., A. Macke, and F. Albers (1999), Effect of crystal size spectrum and crystal shape on stratiform cirrus radiative forcing, *Atmos. Res.*, *52*, 59-75.

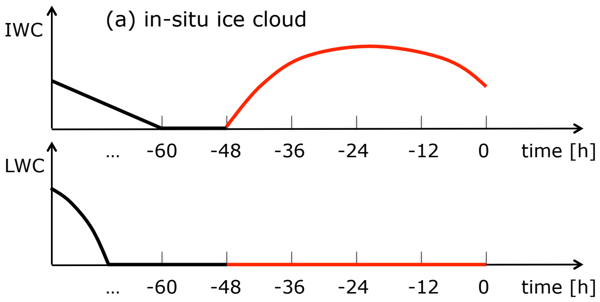

Figure 1. Schematic showing the time evolution of IWC and LWC along backward trajectories from time 0 to beyond -60 hours, for (a) an in-situ ice cloud and (b) a liquid-origin ice cloud. In (a) the considered ice cloud formed at time -48 hours and between this time and $t = 0$ no LWC is present in the air parcel. In (b) the ice cloud formed also at time -48 hours but in this case LWC occurs between -48 and -24 hours.

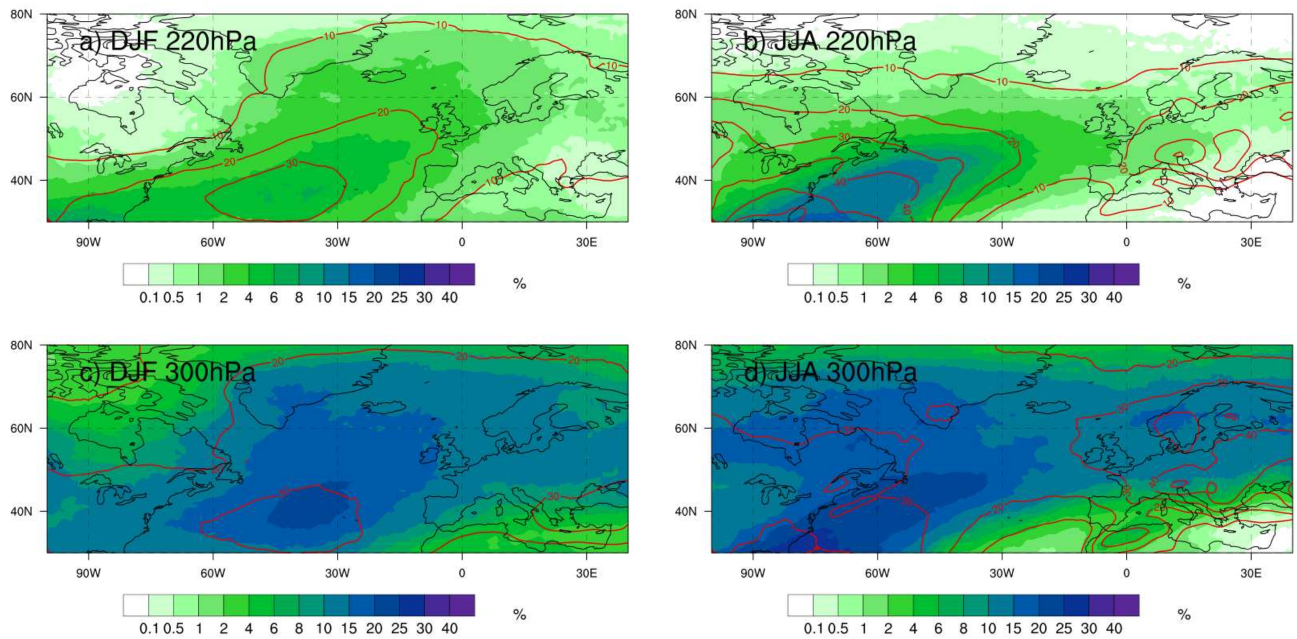

Figure 2. Climatological distribution of in-situ and liquid-origin ice clouds in DJF (left panels) and JJA (right panels) on 220 hPa (upper panels) and 300 hPa (lower panels). Colors show the frequency of liquid-origin ice clouds (in %) and red contours the frequency of in-situ ice clouds (from 10%, every 10%).

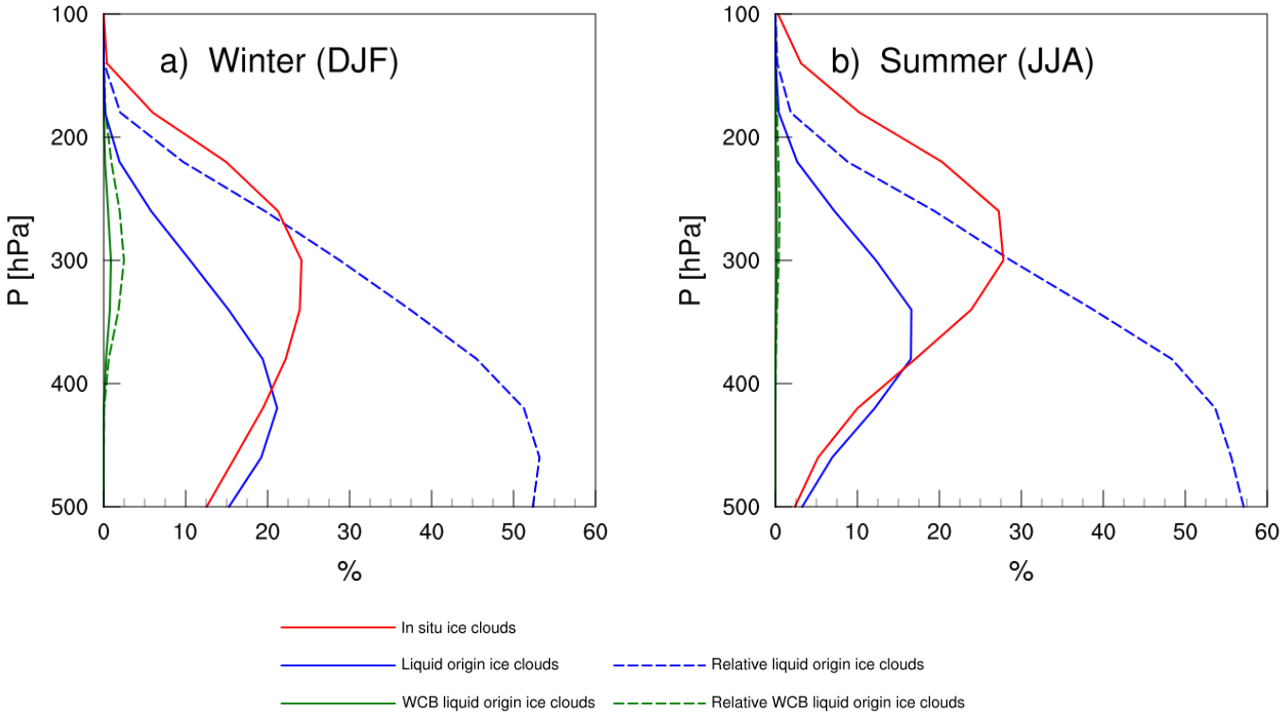

Figure 3. Vertical profile of the climatological distribution of in-situ and liquid-origin ice clouds, horizontally averaged in the domain shown in Fig. 2, for (a) DJF and (b) JJA. The red line shows the frequency of in-situ cirrus, the blue line of liquid-origin cirrus, and the green line of liquid-origin cirrus with WCB ascent, respectively. The blue and green dashed lines show the relative frequency of the last two categories, respectively.

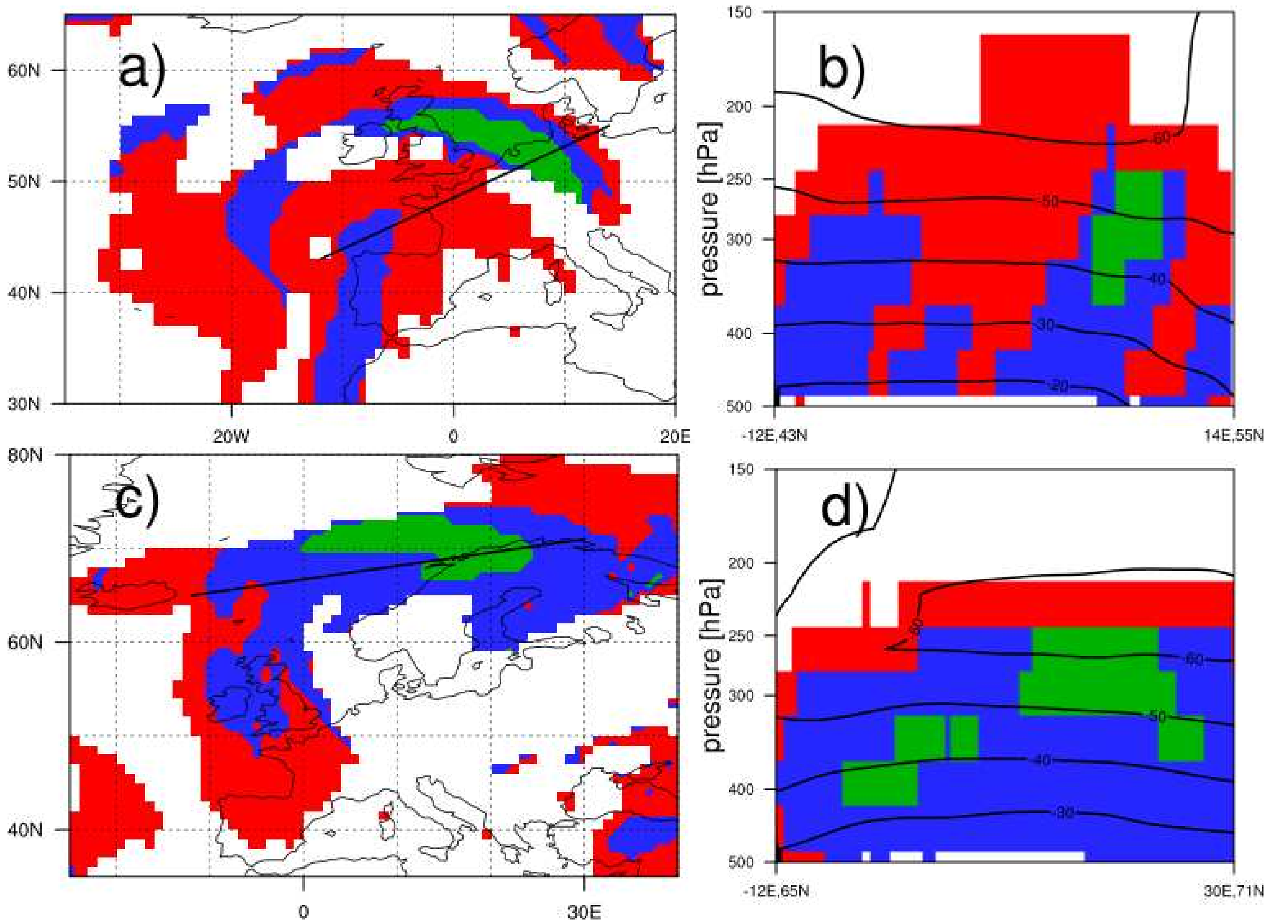

Figure 4. Two case studies of ice clouds over Northern Europe, at 00 UTC 28 November 2000 (upper panels) and 00 UTC 31 January 2009 (lower panels). Colors indicate in-situ origin (red) and liquid-origin cirrus (blue), and the subcategory of WCB-related liquid-origin cirrus (green). Left panels show ice clouds at 300 hPa; right panels vertical cross sections between 500 and 150 hPa along the black lines indicated in the left panels. Black lines in the right panels show temperature (in °C).